ENVIRONMENTAL RESEARCH
LETTERS

LETTER • OPEN ACCESS

The first global catalogue of gas flaring sources derived from a multi-temporal time series of OLI and MSI daytime data: the DAFI v2 algorithm

To cite this article: Mariapia Faruolo *et al* 2024 *Environ. Res. Lett.* **19** 114053

IOP Publishing Environ. Res. Lett. 19 (2024) 114053 https://doi.org/10.1088/1748-9326/ad82fb

ENVIRONMENTAL RESEARCH
LETTERS

OPEN ACCESS

RECEIVED
10 April 2024

REVISED
23 September 2024

ACCEPTED FOR PUBLICATION
3 October 2024

PUBLISHED
14 October 2024

LETTER

The first global catalogue of gas flaring sources derived from a multi-temporal time series of OLI and MSI daytime data: the DAFI v2 algorithm

Mariapia Faruolo[1,2,*], **Nicola Genzano**[3], **Nicola Pergola**[1,2] **and Francesco Marchese**[1,2]

[1] Institute of Methodologies for Environmental Analysis—National Research Council, Tito Scalo, Italy
[2] Space Technologies and Application Centre, Potenza, Italy
[3] Department of Architecture, Built Environment and Construction Engineering—Politecnico Milan, Milan, Italy
[*] Author to whom any correspondence should be addressed.

E-mail: mariapia.faruolo@cnr.it

Keywords: daytime gas flaring detection, global gas flaring catalogue, Landsat 8/9 OLI, Sentinel-2 MSI, DAFI system, temporal monitoring of GF locations and activities

Abstract

Gas flaring (GF) is an industrial phenomenon requiring a special attention for the serious impacts on environment, climate and human health. To analyses and map GF sites (GFs), the Daytime Approach for GF Investigation (DAFI), which is based on daytime data from the Operational Land Imager (OLI) aboard the Landsat-8 satellite, has recently been developed. The GFs catalogue from the DAFI system, spanning over the years 2013–2021, represents the first worldwide GF product generated from mid-high spatial resolution data (30 m). The DAFI version 2 (v2), also including information from the Multispectral Instrument (MSI) aboard Sentinel-2 satellites, already showed an improved capacity in the mapping of GFs over Iran and Iraq. In this work, the new catalogue arising from the porting of DAFI v2 at global scale is presented and discussed. By using a parallel workflow, based on a loop tiling scheme running in Google Earth Engine, DAFI v2 allowed us to extend the GF inventory globally up to 2023, by analyzing ∼4 million of OLI/OLI-2 (Collection 2) and MSI imagery. Results of this study show: (i) an increased DAFI v2 capacity, of about 41%, in detecting GFs compared to the previous DAFI version; (ii) a downward trend (∼4.6%) in terms of GF sites detected from 2021 to 2023. These findings demonstrated that DAFI v2, which will also include the estimates of radiative power at different spatial scales, may contribute in assessing and monitoring the GFs activities and in evaluating the effectiveness of the greenhouse gas-emission reduction strategies at global, continental, national and local scales.

1. Introduction

The gas flaring (GF), i.e. the burning of natural gas associated with oil extraction, is a relevant phenomenon requiring a special attention for the serious global environmental impacts (Emam 2016, Fawole *et al.* 2016, Anejionu 2019, Caseiro *et al* 2020, Faruolo *et al* 2021, IEA 2023). According to the last International Energy Agency report, the GF has been responsible for 500 Mt CO_2 equivalent greenhouse gas (GHG) emissions in 2022, mostly (∼70%) coming from gas flares operating on a near continual basis (IEA 2023). Oil and gas operations alone contribute nearly a fifth of the global methane emissions from human activity, with about half of them occurring in developing countries (World Bank GGFR 2023).

During the 28th meeting of the Conference of the Parties (Dubai, United Arab Emirates, December 2023) (UNFCC 2023), which focused on fast-tracking the energy transition and slashing emissions before 2030, two key GF-related initiatives were launched: the Oil & Gas Decarbonization Charter and the Global Flaring and Methane Reduction (GFMR). Both initiatives were proposed to support the developing countries speed climate action and achieve high-scale impact across the oil and gas sectors by

reducing the carbon dioxide and methane emissions from the oil and gas industry (IEA 2023, UNFCCC 2023, World Bank 2023, GFMR 2024).

To assess the progress of the GFMR initiative, an independent, up-to-date and comprehensive baseline of the global GF sites, at a detailed spatial resolution, is required to monitor countries' energy decarburization efforts, along with their effective implementation (Hu *et al* 2023, Liu *et al* 2023).

Remarkable progress was recently achieved by using multi-platform satellite data to retrieve qualitative/quantitative information about GF sources in terms of location, emission and temporal trend (Faruolo *et al* 2021, 2022a, 2022b, 2023, Liu *et al* 2021, 2023, Wu *et al* 2022, Asadi-Fard *et al* 2023, Caseiro and Soszyńska 2023, Chakraborty *et al* 2023, Elvidge *et al* 2023, Hu *et al* 2023).

The crucial role of satellite systems in this application domain (Onoda and Young 2017, Dubovik *et al* 2021) is likely to be a consequence of the growthing interest of the political agendas as well as of the full, open and free access to extended Earth observation datasets. They are currently summed to a total of 807 PB, increasing by >100 PB per year (Wilkinson *et al* 2024), which may be processed/managed using powerful cloud-based computing systems and platforms, such as Google Earth Engine (GEE) (Gorelick *et al* 2017, Kumar and Mutanga 2018).

A critical review of satellite-based methods developed to study the GF dates to 2021 (Faruolo *et al* 2021).

By analyzing science databases in years post 2021, authors found that the new published papers suggested the use of daytime satellite data to investigate the GF sources, mostly observed, in the past, through nightlight-only images (Faruolo *et al* 2021). In night-time, hot targets are better detectable in the 0.7−2.2 μm spectral range. Two algorithms were then proposed to detect and monitor natural GF and industrial sites using Visible Infrared Imaging Radiometer Suite (VIIRS) (Elvidge *et al* 2023) also analyzing light emission signals (Chakraborty *et al* 2023). The latter is more suited to identify weaker gas flares which are generally undetectable in the thermal bands. The generated GF products are, however, based on satellite data at coarse spatial resolution (i.e. 750 m), which are less suited for an accurate localisation and mapping of GF sources. Indeed, those thermal anomalies, having very high temperatures, usually occupy a small portion of the pixel (i.e. less than 100 m^2) (Faruolo *et al* 2021, Hu *et al* 2023). Although distinct and independent, GF sites (GFs) may be a few tens/hundreds of meters apart and therefore cannot be resolved with low spatial resolution products, like those offered by the VIIRS-like sensors (Wu *et al* 2022). This suggested the use of multispectral imagery, at higher spatial resolution, provided by sensors such as Operational Land Imager (OLI) and Multispectral imager (MSI), respectively aboard Landsat 8/9 (L8/9) and Sentinel 2 (S2) satellites. The higher spatial detail offered by those data allows for a more accurate localization and mapping of GF sources (Faruolo *et al* 2022b). This condition becomes relevant to improve the estimates of GHG emissions and for better evaluating their impact on the environment. In case of GF sites close to the urban contexts or regions deeply affected by their presence, an accurate discrimination of the single system may be crucial to provide data capable of better supporting the management and control of GF sources.

Table 1 lists, in chronological order, the main literature studies focusing on GF investigation by those observations.

The main problem in using daytime MSI and OLI data is, however, the presence of the solar reflected component, which makes the identification of hot targets particularly challenging. Since the first attempts of using those data to investigate GF sources (Anejionu *et al* 2014, Chowdhury *et al* 2014), research has made giant strides in this direction, making available high-quality satellite-based products suited to detect, map and monitor GF sites (onshore and/or offshore) at local, national or global scale (Liu *et al* 2021, Hu *et al* 2023). Among the systems, we recently developed an open access platform, operating on daytime imagery to complement the global nighttime VNF (VIIRS NightFire) dataset (https://eogdata.mines.edu/products/vnf/subscribers/index.html) (Elvidge *et al* 2013, 2016, Zhizhin *et al* 2021). The system, named Daytime Approach for GF Investigation (DAFI) (Faruolo *et al* 2022b, 2023), is freely accessible online (https://sites.google.com/view/flaringsitesinventory).

DAFI, which is a GEE-based application, by analyzing multi-temporal series (2013–2021) of L8 OLI radiances, has provided the first global high-resolution catalogue of high-temperature GFs, which was updated to 2021 (Faruolo *et al* 2022a, 2022b).

Recently, (Faruolo *et al* 2023), we tested a new version of the DAFI system (i.e. DAFI version 2, v2) based on L8/L9 OLI/OLI-2 and S2 MSI data integration over Iran and Iraq, where an increment of the DAFI accuracy in detecting GFs of more than 50% was measured in 2022.

In this study, we propose the porting of DAFI v2 at global scale, and the first map of worldwide GF sources generated through the processing of a multi-sensor system coupling multi-year time series of mid-high resolution daytime satellite data (spanning from 2013 to 2023). More specifically, the 2021 global GFs picture from DAFI v2 is presented, discussing differences with the previously DAFI (v1) map. Besides, we show the updated catalogue of onshore and offshore GFs computed in 2022 and 2023, representing the main findings of this work.

Table 1. Literature papers collected by science databases focusing on daytime gas flaring investigation from space.

Paper	Scale analysis	Satellite sensor(s)	Spectral bands	Time window
This work	Global (offshore/offshore)	OLI/OLI-2 MSI	NIR[a], SWIR1[b]	2013–2023
Hu *et al* (2023)	Local (onshore/offshore)	MSI VIIRS[c]	NIR, SWIR1, SWIR2	2021
Faruolo *et al* (2023)	National (onshore/offshore)	OLI/OLI-2 MSI	NIR, SWIR1	2013–2022
Liu *et al* (2023)	Global (offshore)	MSI	NIR, SWIR1, SWIR2	2015–2021
Asadi-Fard *et al* (2023)	Local (offshore)	OLI	VIS, NIR SWIR1, SWIR2	2018–2019
Wu *et al* (2022)	National (onshore)	OLI MSI	NIR, SWIR1, SWIR2	2013–2022
Faruolo *et al* (2022b)	Global (onshore/offshore)	OLI	NIR, SWIR1	2013–2021
Faruolo *et al* (2022a)	Local (onshore/offshore)	OLI MSI	NIR, SWIR1, SWIR2	2012–2019
Liu *et al* (2021)	Global (offshore/offshore)	MSI	NIR, SWIR1, SWIR2	2016–2018
Chowdhury *et al* (2014)	Local (onshore)	OLI	SWIR1, SWIR2	2013
Anejionu *et al* (2014)	National (onshore/offshore)	TM4-5/ ETM+	NIR, SWIR1, SWIR2	1984–2012

[a] Near Infrared.
[b] Shortwave Infrared.
[c] Nighttime.

2. Data and method

The updated DAFI version (i.e. DAFI v2) integrates the OLI/OLI-2 and MSI observations (up to 20 m spatial resolution). Multi-temporal satellite series of Level-1 OLI (2013–2023, ∼104 TB) and MSI (2015–2023, ∼2.221 TB) observations, consisting of ∼3.8 million imagery, were aggregated in three temporal windows (i.e. 2013–2021, 2013–2022, 2013–2023) and processed using GEE, according to the DAFI requirements (Faruolo *et al* 2022b, 2023).

The main features of the DAFI v2 configuration proposed in this study are:

1. the processing of Collection 2 (C2) in place of Collection 1 (C1) for Landsat OLI data;
2. the synergic use of OLI, OLI-2 and MSI data, which benefits from the increased temporal resolution of the combined L8, L9 and S2 revisit time (up to 2.3 d) (Chaves *et al* 2020, Wulder *et al* 2021);
3. the updating of GF inventory with the 2022 and 2023 data.

The DAFI v2 system uses a Normalized Hotspot Index (NHI_{SWNIR}) (Marchese *et al* 2019, 2022), analyzing the daytime radiances measured in the Near infrared (NIR) and Shortwave infrared (SWIR) bands, and a test for the Extremely Hot Pixels (EP) to select and map GFs (Faruolo *et al* 2022a, 2022b).

Figure 1 displays the DAFI v2 flowchart, showing the in parallel computing workflow introduced by the version 2 (Faruolo *et al* 2023), which is based on a dual step analysis:

1. *hot pixel identification*: the system considers 'hot' each pixel having positive values of the NHI_{SWNIR} over the single satellite scene, analyzed or surveying to the EP test in the SWIR1 band (Genzano *et al* 2020) (HP_{daily}) (see the 'Image Processing' step in figure 1);
2. *gas flare selection*: the system flags as gas flares only the hot pixels having an occurrence frequency (OF) equal or greater than ⩾10% (see the 'Collection Processing' step in figure 1); the OF is calculated as the ratio between the sum of the detected HP_{daily} and the number of satellite imagery available for the investigated period.

As discussed in a previous study (Faruolo *et al* 2022b), DAFI v2 is biased towards GF sources with temperatures $T \geqslant 1800$ K, hence the GF operating at lower temperatures and emitting less in the SWIR1 band could be missed by the system. In addition, DAFI v2 is expected to be less effective in mapping recent (or presently dismissed) plants, which do not meet the used criteria, especially in terms of OF.

For these reasons, the DAFI v2 inherent findings are generally less numerous than other GF datasets, independently derived by using the same satellite data, such as those proposed by Caseiro *et al* (2020) and Liu *et al* (2021, 2023).

Figure 1 shows how DAFI v2 defines a global gas flares dataset ('GF Catalogue Creation'). In each process, a loop tiling scheme (2932 and 3592 tiles for OLI and MSI, respectively) was used to improve the cache performance, reducing the code execution time and controlling over the output quality and size (Ye *et al* 2020). A clustering-based criterion was

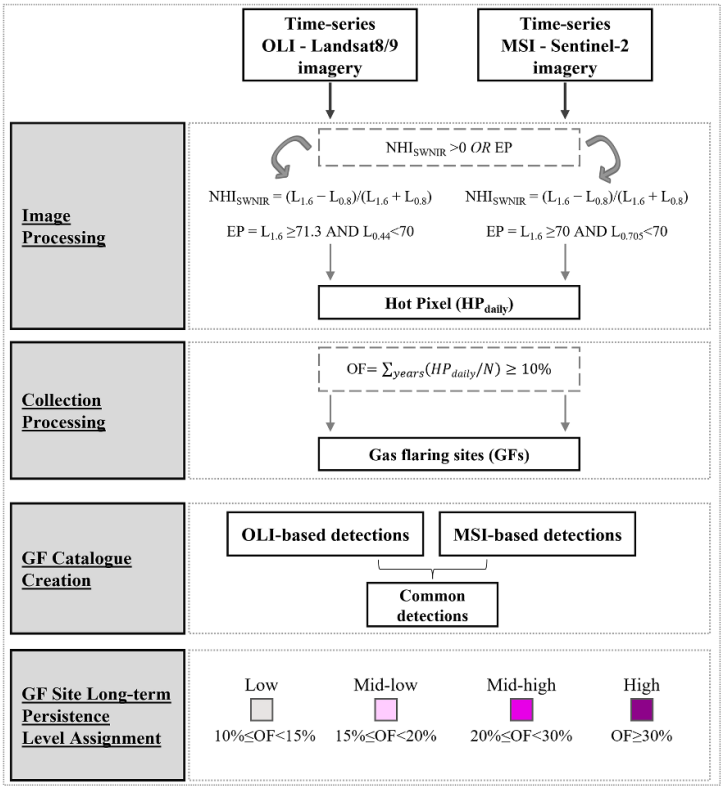

Figure 1. Flowchart illustrating the DAFI version 2 method (DAFI v2).

then applied to extract gas flare locations (i.e. longitude and latitude coordinates) and map the GF affected area. Figure 2 shows an example describing this scheme, in reference to the gas flares located in the southern Iraq and belonging to the Markazia degassing station (Ali *et al* 2017).

Based on the persistence of the GF thermal anomalies, an OF raster map with OF values from 10% to 100% (depicted in different colors; see OF legend in figure 2) is got. Hot pixels in the segmented OF image (red dots, on the top left of figure 2) correspond to the pixels with OF $\geqslant$ 10%. The raster to vector conversion creates a set number of hot pixels: although the GF itself occupies a spatial area within the range of one pixel of the OLI/MSI images, thermal emission from gas flares tends to spread over the surrounding pixels, generating a cluster of hot pixels. Therefore, hot pixels within a 37.5 m (for OLI)—25 m (for MSI) radius (i.e. 1.25 $\times$ pixel size) are assumed to belong to the same GF plant. Dissolving the single buffers allows to map the GF-affected area (cyan vector, on the bottom left of figure 2), while their conversion into geometric centers localizes the GF plant in terms of longitude and latitude (pink and cyan dots, on the bottom left of figure 2). At the end of the process, each yearly GF database is composed of a set of GFs detected by a single sensor (e.g. the two cyan vectors on the top right of figure 2, here detected by MSI only) and by the GFs detected by both sensors (i.e. common detections, the ones where OLI and MSI buffers touching, yellow vector in the example of figure 2, on the top right corner).

Finally, the GF thermal activity of the site is qualitatively described by the long-term persistence level ('GF Site long-term persistence level assignment', figure 1), corresponding to low for 10% $<$ OF $<$ 15%, mid-low for 15% $\leqslant$ OF $<$ 20%, mid-high for 20% $\leqslant$ OF $<$ 30%, high for OF $\geqslant$ 30%. This value depends on the maximum OF recorded within the OLI/MSI buffer; for the common detections the max OF value between the OLI and MSI estimates is chosen to represent the area. The lower this level is, the lower the GF continuity over time.

All findings provided by the DAFI implementation are assumed to be robust, with an associated accuracy of 99% and a negligible commission error equal to 1% (related only to other industrial plants), as previously estimated in (Faruolo *et al* 2022b).

3. Results

The first global map of GFs derived from a multi-sensor system has been produced. It combines OLI and MSI infrared radiances, acquired in between 2013–2023 and 2015–2023 respectively, and operating in daytime conditions at 20/30 m spatial resolution. The achieved results consist of:

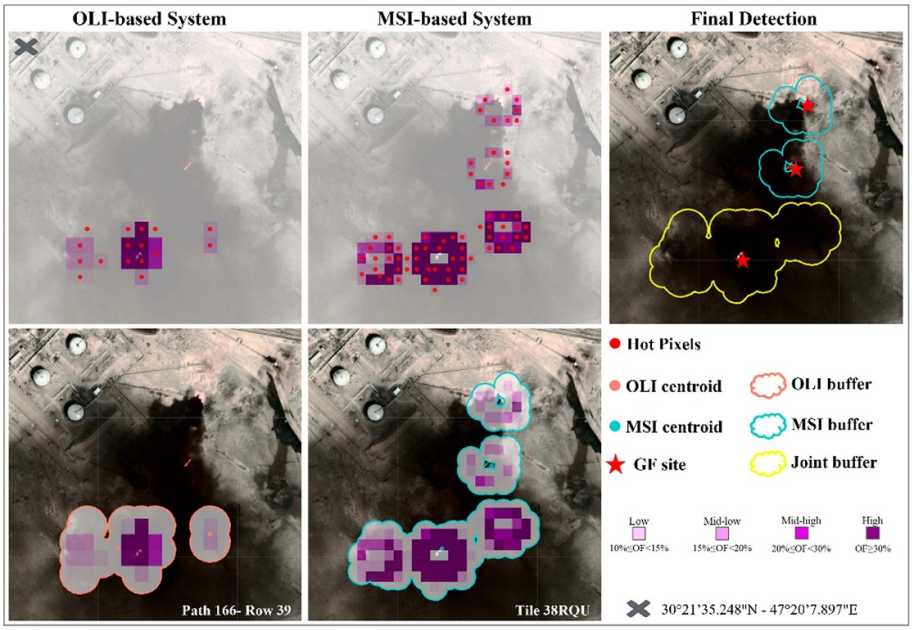

Figure 2. Definition of the spatial aggregation scheme used to localize the gas flares: a red dot is placed in correspondence of pixels with OF $\geqslant$ 10% (on the top left, for OLI and MSI scenes); a dissolved bounding vector (in pink and cyan, on the bottom left, for OLI and MSI, respectively) is placed around the OLI and MSI centroid (pink and cyan dot on the bottom left) to map the GF affected area. The final GF location is defined by centroids (red stars) inherent to the single (the cyan ones) and joint (the yellow one) buffers (on the top right). In background, the Markazia degassing station (Iraq) (Ali *et al* 2017), where three gas flaring sites were identified in 2022, in the OLI path/row 166/39 and MSI tile 38RQU.

(i) the GF global map referring to 2021, generated using the two DAFI versions over the period 2013–2021; the first map, recently shown in Faruolo *et al* (2022b) is based on the L8 OLI C1 while the second one relies on the L8/9 C2 of OLI and OLI-2 data, along with MSI data spanning from 2015 to 2021 (section 3.1);
(ii) the DAFI v2 GF global map updates for the years 2022 and 2023 (section 3.2).

3.1. DAFI v1 vs DAFI v2 maps at 2021

To assess the performance of DAFI v2, we performed a comparison with the results previously achieved by using the DAFI v1 approach. Figure 3 displays the GF locations identified by DAFI v2 (purple dots) and DAFI v1 (green dots) over the same period, spanning from 2013 to 2021. An inventory of 2419 gas flares at the global scale was established by DAFI v2, whereas DAFI v1 identified 1711 GF sites, with a 41% increasing in GF detection. The latter, which is marked by the yellow circles with purple dots in figure 3, are mainly located in Asia (39%), Africa and Europe (23% each one), and are hosted (in decreasing order) by Nigeria, Russia, China, Iran, Iraq, Venezuela and Malaysia; they account for 52% of new GFs.

With reference to figure 3, the GFs geographic distribution (including the onshore-offshore location) remained almost unchanged as far as DAFI v2 is implemented, whereas an upward trend was observed in Africa and Asia (10% and 5%, respectively) and a downward one in the rest of the world (Americas: −13%, Oceania: −10%, Europe: −5%).

The improvements shown by the updated DAFI version are emphasized, in a qualitatively/quantitatively way, by the investigations performed over the regions of Russia, Algeria, Iraq and Iran (i.e. areas identified by the black boxes in figure 3) shown in the insets of figure 4.

More in general, as far as the global scale is considered, the scheme in figure 5 highlights the differences in the number of GFs for 2021 characterizing the single (DAFI v1) and dual sensor configuration (DAFI v2),

Regarding the DAFI v2 of the 2419 total detected gas flares, 63% of them (1534 sites, figure 5) were observed by both MSI and OLI. The agreement of results retrieved from two independent processing chains strengthens the reliability of the used detection scheme. Along with the common detections, the single sensors enabled the unique identification of a not negligible number of GF sites. Indeed, 14% of the new sites were only identified by OLI while 23% by MSI (i.e. 340 GFs for OLI and 545 for MSI).

Furthermore, the analysis of the C2 OLI/OLI2 datasets over the period 2013–2021 (the same of the DAFI v1), allowed us to identify 1832 GFs, with an increment of 7% in the number of sites (1711), which were previously recognized using the C1 OLI collection (Faruolo *et al* 2022b). The reason of this improvement is twofold: (i) the higher number of available satellite scenes, those from L9 OLI2

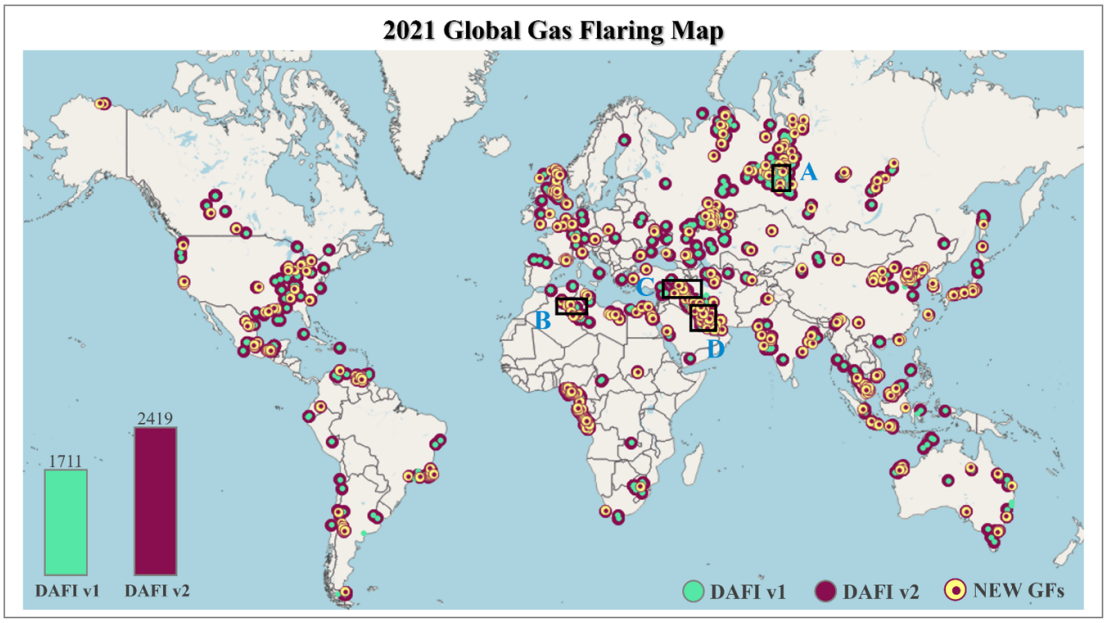

Figure 3. Gas flaring scenario at 2021 according to DAFI v1 (green dots) and v2 (purple dots) by processing 2013–2021 images. The yellow circles with purple dots highlight the new GFs detected by DAFI v2. The black boxes are used in following analyses.

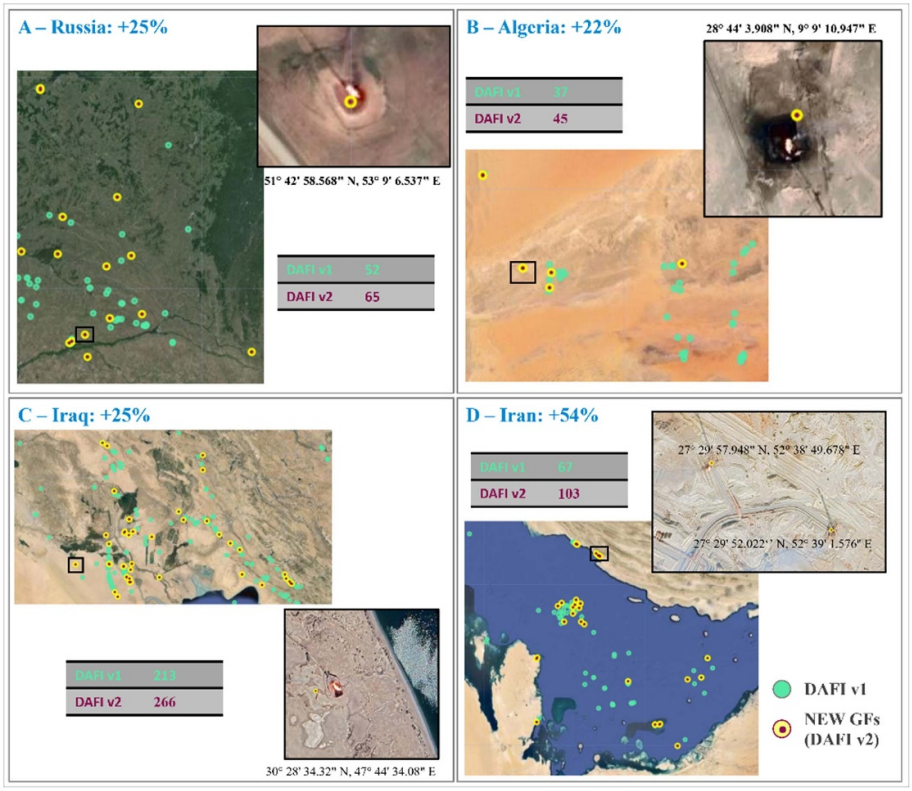

Figure 4. Magnification of the areas marked by the black boxes in figure 3 showing the DAFI v2 improvements in comparison with the DAFI v1. Green numbers and dots are DAFI v1 detections, whereas DAFI v2 new identifications are depicted as yellow circles with purple dots (as in figure 3) and quantified by the purple numbers.

allowed for a more frequent temporal sampling and a higher probability of clear-sky observations; (ii) the increased accuracy in terms of data quality of C2 compared to C1. In detail the C2 offers a substantial improvement in the absolute geolocation accuracy, thanks to the updated digital elevation modeling

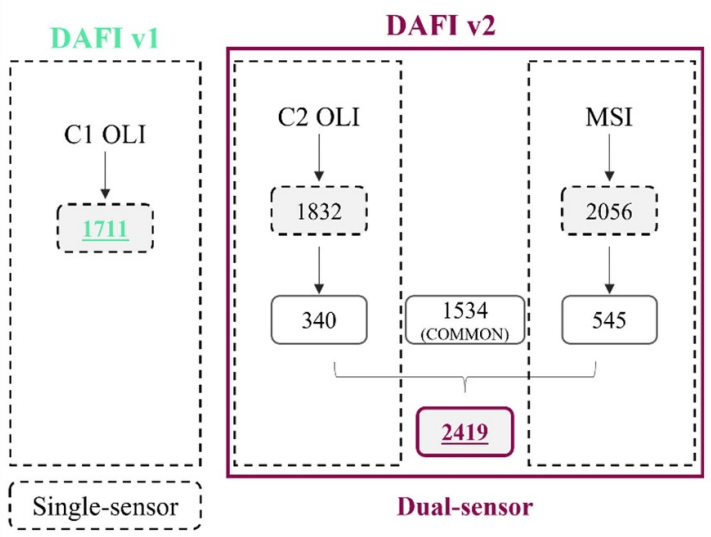

Figure 5. Number of gas flares detected in 2021 by DAFI v1 and v2, with the single- and dual-sensor based GF detections.

sources, an improved radiometric calibration, and an enhanced quality assessment band (Masek *et al* 2020, USGS 2020, Micijevic *et al* 2022).

The stability of point positions over time and the higher frequency of observation may improve the results of the multi-temporal analyses. Concerning the DAFI v1, the lower geolocation accuracy probably leaded to an error in the computation of OF values, with a consequent underestimation of some potential gas flares. On the other hand, the higher quality of C2 OLI data allowed us to reduce the omission errors, improving the general DAFI sensitivity and accuracy. This is demonstrated, for instance, by the correct identification of the GF site located in Algeria, within the Hassi R'Mel oil&gas field (Naus *et al* 2023) (see gas flare at Lon 3.234592E, Lat 32.93589N-path/row 195/37 OLI tile in figure 6), which were undetected by using the C1 L8 dataset. Besides, the joint usage of C2 OLI data and MSI imagery increased the DAFI detection sensitivity, thanks to the higher spatial resolution and to an improved revisit time, as widely verified in a previous study (Faruolo *et al* 2023). This allowed us to identify new 545 gas flares (see, for example, the gas flare at Lon 6.70942E, Lat 32.513001N and the OF values for 32SKA MSI tile and path/row 193/37 OLI tile reported in figure 6).

While the exclusive MSI detections are ascribable to the higher spatial resolution of MSI than OLI data, the OLI-based have caught the author's attention. Figure 6 shows some examples of gas flares identified only by OLI; all the marked sites correspond to real oil and gas plants, as stated in previous studies referring to GF activities practiced in Algeria (figure 5(a), Flareintel 2021), Egypt (Figure 6(b), Carbon Limits AS 2016), Russian Federation (Figure 6(c), Böttcher *et al* 2021). In these cases, the MSI-based OF estimations are lower than the used fixed threshold (10%), and this may occur owing to: (i) gas flares operating intermittently or for a short period during the considered time span (2015–2021); (ii) less intense thermal sources undetectable by the used NHI-based detection scheme (see the charts at the bottom of figure 6).

3.2. Global GF daytime maps from 2021 to 2023

The DAFI v2 detection scheme has been implemented to update the global daytime GF map to the most recent 2022 and 2023 years. Figure 7 displays the status of gas flares distributed all over the world from 2021 to 2023, along with the detail of single and dual sensor-based detections computed for each investigated period.

Figure 7 shows a quite stable scenario in terms of detected gas flares from 2021 ($n = 2419$) to 2023 ($n = 2308$), with a slight GFs decline of ∼2.4% from 2021 to 2022, and of ∼2.2% from 2022 to 2023. Differences between the three maps are minor, with only some 2021 GF site disappearing in 2022 and/or in 2023 (e.g. Lon 71.499074E-Lat 25.92984N, India). On the other hand, only a few additional GF sites established in 2022 and/or 2023 (e.g. Lon 37.868313E-Lat 59.148556N, Russia).

An in-depth analysis of the output from DAFI v2 revealed that the GF status of 2021 remained mostly unchanged in the following two years, both in terms of spatial distribution by continent (Asia: ∼41%, Europe: ∼22%, Africa: ∼18%, Americas: ∼16%, Oceania: ∼2%) and onshore/offshore localization (∼70% onshore and ∼30% offshore). All the GFs belong to 77 countries, with 10 countries that were responsible for the 62% of total GF detections

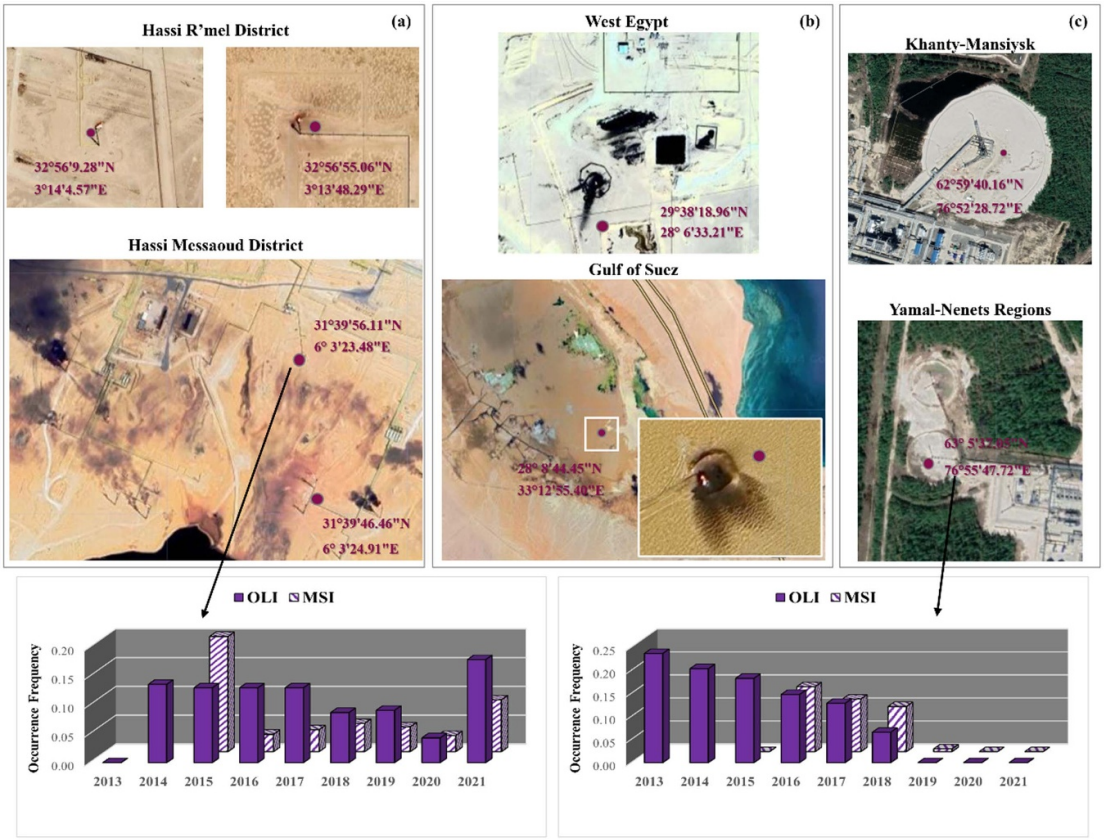

Figure 6. Examples of OLI-only GF detections in 2021 randomly selected around the world. The charts at the bottom refer to the two gas flares selected to show the possible causes of MSI missed detections.

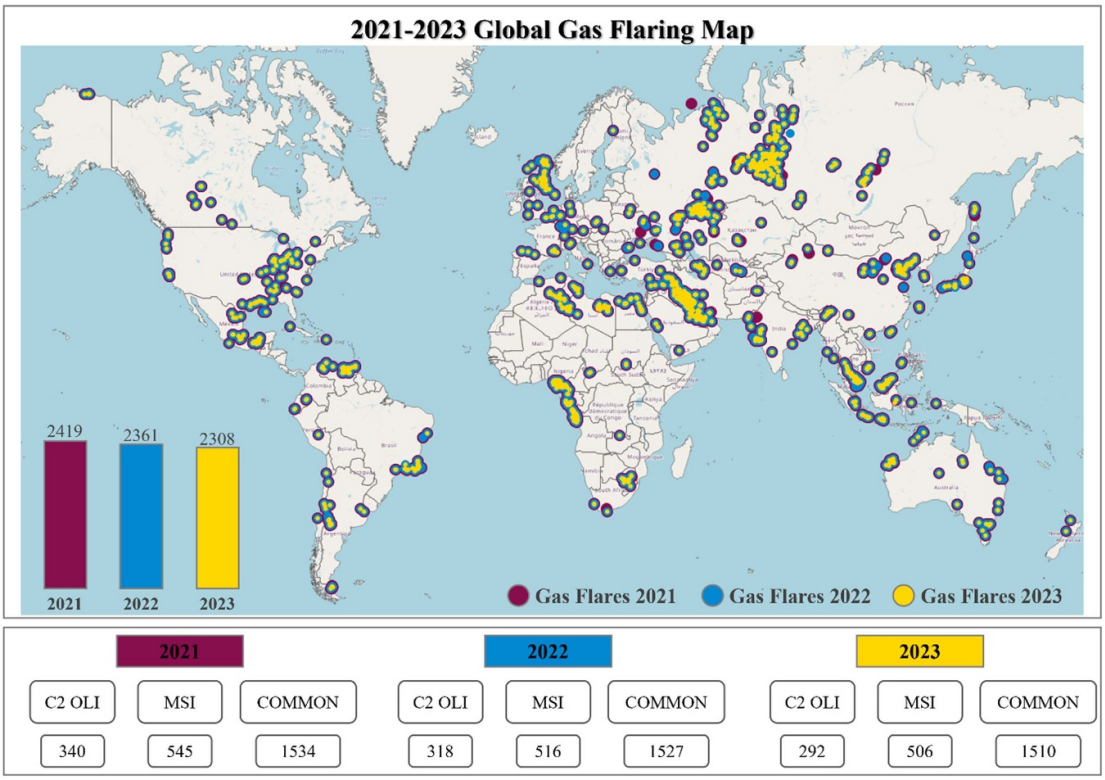

Figure 7. Worldwide gas flares evolution retrieved over the period 2021–2023 through the DAFI v2 implementation. Results from the dual sensor approach in terms of common (C2 OLI and MSI) and unique (C2 OLI or MSI) detections for each investigated temporal period are summarized in the boxes under the map.

Table 2. GFs changes from 2021–2022–2022–2023 from literature papers collected by science databases focusing on daytime gas flaring investigation from space.

GFs change	2022–2023		
2021–2022	up	down	unchanged
up	5%	4%	5%
down	6%	18%	12%
unchanged	8%	6%	35%

over the period 2021–2023, i.e. Russia (17%), Iran (9%), Iraq (9%), China (5%), Nigeria (4%), Algeria (4%), Mexico (4%), Venezuela (3%), United States (3%) and India (3%). In detail, Russia, Iran and Iraq are the top three countries in terms of GF for the entire studied period (World Bank 2023), representing ∼50% of the total gas flares identified onshore; gas flares operating offshore are mostly located in the Persian Gulf and South China Sea (48%), followed by the Gulf of Guinea (26%), the Gulf of Mexico (11%) and the North Sea (11%) (Liu *et al* 2023).

A continuous increment in the number of GFs identified from 2021–2022–2022–2023 was recorded by DAFI 2 for Iraq, Japan, Libya and Mexico, accounting for the 5% of GF affected countries (table 2). The trend is reversed in 18% of countries (i.e. Algeria, Angola, Argentina, Australia, China, Denmark, India, Indonesia, Norway, Romania, Russia, Ukraine, United Kingdom Uzbekistan).

It is worth noting that the GFs remained unchanged over time in about 35% of the countries.

3.3. Summary and discussion

This paper presents a global database of GFs, the first one created by using a multi-sensor satellite-based approach, the DAFI v2, a conceptually simple and efficient system for GF detection and monitoring, based on the joint processing of more than 10 years of both OLI and MSI daytime imagery. This catalogue is not immune from limitations and uncertainties, due to both the highly variable nature of GF and the multiple factors influencing the detection accuracy (e.g. spatial coverage and temporal resolution of satellite imagery, missing value pixels in some regions, background contamination). However, despite those uncertainties, the proposed GF database has demonstrated to be robust, with a reliability of about 99%, as estimated in a previous work (Faruolo *et al* 2022b), and more accurate than the previous database generated using only C1 OLI data. Indeed, this study shows that DAFI v2 has significantly improved the original DAFI v1 detection capability on a global scale, increasing of 41% the number of worldwide high-temperature gas flares.

The new global GF dataset updated to 2023 reveals a slight downward trend in the GF sources, with a ∼4.6% reduction from 2021 to 2023. When paired with the GF-related information included in the last GGFR report (World Bank 2023) some useful considerations arise. Table 3 resumes the alignment/misalignment between GF sites change over the period 2021–2022 and the variation in the gas flared volumes (Billion Cubic Meters, BCM) provided by SkyTruth (https://viirs.skytruth.org/apps/heatmap/flarevolume.html), both aggregated at the country level. The nine countries responsible of 74% of BCM in 2022 according to the GGFR were targeted.

Table 3. A country-level estimation of DAFI v2 GF detections and gas-flared volumes changes recorded over the period 2021–2022. The colors represent the increasing (up), decreasing (down, in bold) or stable (in italics) trend.

2021–2022 change	GFs DAFI v2	BCM
Russia	down (−3%)	down (−1%)
Iraq	*stable*	*stable*
Iran	down (−2%)	down (−1%)
Algeria	down (−5%)	up (+3%)
Venezuela	down (−7%)	up (+7%)
United States	down (−7%)	down (−9%)
Mexico	*stable*	down (−13%)
Libya	up (+21%)	down (−9%)
Nigeria	*stable*	down (−18%)

Table 3 shows that Russia, Iran and United States exhibited a declining trend from 2021 to 2022 in both metrics. These countries along with Nigeria and Mexico accounted for most of the decline in global GF recorded in 2022. Indeed, in front of an unchanged number of GFs, the World Bank reported a significant reduction in the GF volumes of 18% and 13% for Nigeria and Mexico, respectively. In Iraq, the stable situation was marked also by DAFI v2. Regarding the Algeria and Venezuela, the DAFI v2 unlike the BCM marked a reduction of gas flares. In Libya, there is a mismatch between the increasing trend in the number of GFs and the emitted volume reduction marked by the BCM. Despite those differences/similarities, table 3 shows that information from different sources/methodologies may represent a remarkable benefit. The merging of independent information might provide a better picture of the current state of a phenomenon that, despite the existing policies devoted to its reduction/elimination, still represents a serious concern.

The DAFI implementation on OLI and MSI data shows a dual benefit. Specifically, a set of gas flares was detected only by OLI or MSI, whereas both sensors observed other GFs. The latter corroborate the single detections, while the single sensor implementation assured an add-on value to DAFI v2. This includes the recovery of gas flares that were unresponsive within the twin system because of several limitations, such as the temporal persistence of thermal anomalies, the weather conditions at the overpass time, and most importantly the highly variable nature of GFs. Although the gas flares can be considered as persistent hot sources in both time and space, the GF activity

Table 4. Main features of nighttime and daytime methods used to detect gas flaring sites and compared in this work.

Reference paper	Satellite sensor (spatial resolution)	Temporal frequency	Primary GF detection bands	GF temperature range [K]	GF selection filter on single image	GF discrimination strategy	Temporal basis
Elvidge *et al* (2013, 2016)	VIIRS (750 m)	Daily	DNB, NIR, SWIR1, MIR	1000−2600	SWIR, NIR, MIR radiances > threshold	average T > 1600 K & detection in at least 20% of the cloud-free observations	Year
Caseiro *et al* (2020)	SLSTR (500 m)	Daily	SWIR, MIR, TIR	>1500	SWIR, NIR, MIR radiances > threshold	maximum T > 1500 K & hotspot persistency > 5	Year
Liu *et al* (2021, 2023)	MSI (20 m)	5 d (S2A + S2B)	SWIR1, SWIR2, NIR	1200−2200	Tri−spectral reflectance index > threshold	OF (TAI[a]⩾1) ⩾ 10	Multi−year
This work	OLI/OLI2/MSI (30/20 m)	up to 3 d (L8 + L9 S2A + S2B)	SWIR1, NIR	>1800	Bi−spectral radiance index > threshold	OF (NHI_{SWNIR} > 0 OR EP) ⩾10%	Multi−year

[a] Thermal Anomaly Index.

can be interrupted for some periods or the intensity reduced, modifying the pixel spectral behavior in the SWIR and NIR bands. In presence of a dense and quite persistent cloud cover masking the underlying hot target, the GF activity can be totally or partially missed. The joint use of the Landsat 8/9 and Sentinel-2A/B platforms, as a virtual constellation, guarantees a significant improvement in terms of temporal resolution, which may be suited to overcome some of these drawbacks and better optimize the GF investigation.

All these findings can be visualized and explored through the DAFI v2 GEE Apps, hosted in the website https://sites.google.com/view/flaringsitesinventory, allowing the user to achieve a full analysis of the GF activity at the site-level, by visualizing the GF site thermal fluctuations over the years and/or months.

While the proposed global inventory is not exhaustive, DAFI is focused on the selection of the very high-temperature gas flares (those with the emission peak at 1.6 μm) representing a major achievement. DAFI v.2 provides the first open industrial GF heat sources map identified through satellite daytime imagery at mid/high spatial resolution. Additionally, DAFI v2 will account also for the thermal characterization of gas flares. Specifically, the radiative power computation is going to be included in the processing chain and will be used to retrieve the gas flared volumes and GHG emissions, at both global, country and site level.

DAFI v.2 will then provide quantitative information about the GF environmental impacts, contributing to assess the efficiency of the policies and strategies devoted to the GF reduction.

It is important to remark that the DAFI v2 approach was developed to detect only gas flares persistent in time (i.e. with a temporal persistence computed over 11 and 8 years, for OLI and MSI, respectively, OF > 10%) (see figure 1). This makes DAFI v2 robust and accurate although the GFs number are lower than those provided by other datasets operational in both nighttime (e.g. Elvidge *et al* 2013, 2016, Caseiro *et al* 2020) and daytime (e.g. Liu *et al* 2021, 2023). Table 4 summarize the main features of each considered algorithm/system.

Table 5. GF detections provided, at global scale, by nighttime methods in 2017 (source: Caseiro *et al* 2020) vs DAFI v2 findings in 2013–2021.

Night vs Day				
	Method	Investigation year	Observational conditions	Detected gas flares
Globally	VNF	2017	Nighttime	10 185
	SLSTR-based method	2017	Nighttime	6232
	DAFI v2	2013–2021	Daytime	2419

As shown in table 4, the methodological steps (i.e. GF selection filter and discrimination strategy) used to identify gas flares, coupled with the investigated spectral range and the space-time resolution of each data, are different. The nighttime methods analyze both temperature and persistence of a defined GF discrimination parameter, computed throughout a single year, to distinguish gas flares from other hot targets. The daytime ones exploit the persistence of a spectral index computed over a long-term period. These heterogeneous features indicate different GF types and consequently lead to different method results. To better understand these differences, we performed a quantitative comparison among all GF-related findings mentioned in table 4 (see tables 5–7).

The nighttime GF detections provided by VNF and the SLSTR-based method (Caseiro *et al* 2020) are significantly higher than those from DAFI v2 (table 5). In absence of the solar component, data collected at night in the NIR and SWIR spectral bands are affected by the background noise, while

Table 6. Top five GF countries according to methods listed in table 4.

VNF	SLSTR-based method	DAFI v2
United States	Russia	Russia
Russia	United States	Iran
Canada	Iran	Iraq
China	China	China
Iran	Algeria	Nigeria

Table 7. Offshore GFs identified by two daytime algorithms over a long-term period (source for TAI data: Liu *et al* 2023).

	Day vs Day		
	Method	Investigation year	Detected gas flares
Offshore	TAI-based method	2016–2021	1718
	DAFI v2	2013–2021	740

high radiant emissions characterize the pixels containing combustion sources, such as a gas flare, biomass burning, or hot lava. This favors the identification of gas flares, as indicated by the VNF- and SLSTR-based detections which are respectively 4 and 2.5 greater than the DAFI v2. However, a general spatial agreement among the three methods is evident when the GF maps are visually compared at continent/country level (see figure 18 in Caseiro *et al* 2020 and figure 7 in this work). By analyzing data provided by Caseiro *et al* (2020) for 2017, 3 countries among the 5 top GF-affected are common to the methods (table 6). In detail, the general consistency between VNF/SLSTR-method global findings and VNF/DAFI ones was demonstrated by Caseiro *et al* (2020) and Faruolo *et al* (2022b), respectively. This reinforces the potential of each system in detecting GFs, suggesting their integration. As demonstrated by Caseiro *et al* (2020) and Faruolo *et al* (2022b) for nighttime (SLSTR, at 500 m) and, especially daytime (e.g. OLI and MSI at 30/20 m) observations, a spatial resolution higher than VIIRS (750 m) enables the identification and quantitative characterization of small-scale gas flares (Caseiro *et al* 2020) and the accurate localization and mapping of the area affected by the GF phenomenon (Faruolo *et al* 2022b). This accuracy is an add-on value when a detailed characterization of the site, in terms of gas flared volumes and GHG emissions, especially at regional/local scale, is required (Caseiro *et al* 2020, Faruolo *et al* 2022b, Liu *et al* 2023).

The daytime TAI and NHI related products (table 7) derive from similar discrimination strategies (table 4), although they differ in absolute terms. A lower sensitivity of DAFI v2, with almost the 43% of TAI-based detections, is recorded in marine zones investigated by Liu *et al* (2023). This may be explained considering the selective detection conditions chosen by DAFI, including: (i) a narrower range of source temperatures (>1800 K), and (ii) the stringent threshold used to identify very hot persistent pixels. Nevertheless, DAFI, unlike the TAI-based approach, has been implemented at global scale and is currently providing GF distribution worldwide.

Additionally, DAFI-2 identifies single GFs that remain undetected by other approaches. It appears more performing than TAI over the Yellow Sea, where the latter does not pinpoint operational platforms (see figure 1 in Liu *et al* 2023). Moreover, DAFI-2 is less affected by factors causing false identifications, unlike the SLSTR-based method. The latter mis-classifies, as high-accuracy hotspots, the Etna (South Italy) and K-lauea (Hawaii) volcanoes as GF sources, as evident by looking at figure 8 in Caseiro *et al* (2020), while it does not identify an actual GF site (i.e. the Italian oil & gas plant located in Basilicata region, see Faruolo *et al* 2014, 2020).

In summary, in absence of global ground-truth data on GFs, all satellite-driven products become a useful tool to recover information on GF presence, activity, magnitude and persistence. This suggests their integration for a more comprehensive detection and characterization of the phenomenon at local/regional/global scale. The complementarity and consistency of multi sources satellite products operating in different observational conditions may allow for the development of a single, integrated observational system. The latter would increase the transparency and accuracy levels in the GF monitoring and characterization (Caseiro *et al* 2020, Caseiro and Soszyńska 2023, Faruolo *et al* 2023). This integration may contribute to the GHG reduction strategies and the Paris Agreement goals. In this context, high quality, detailed and low bias products, such as those here presented and discussed, could support the activities of international initiatives and programs (World Bank GGFR/GMFR, Copernicus Atmosphere Monitoring Service, International Energy Agency).

Data availability statement

All data referred to DAFI v2 can be found at https://sites.google.com/view/flaringsitesinventory.

ORCID iDs

Mariapia Faruolo https://orcid.org/0000-0001-5291-8241
Nicola Genzano https://orcid.org/0000-0001-8184-5635
Nicola Pergola https://orcid.org/0000-0001-7619-6685
Francesco Marchese https://orcid.org/0000-0001-7590-5638

References

Ali K K, Husain H A and Shafik Sh S 2017 NORM in markazia degasing station within North Rumaila OilfieldSouthern Iraq *Iraqi J. Sci.* **58** 1464–76

Anejionu O C D 2019 Rationale, historical developments and advances in remote sensing of gas flares *Int. J. Remote Sens.* **40** 6700–19

Anejionu O C D, Blackburn G A and Whyatt J D 2014 Satellite survey of gas flares: development and application of a Landsat based technique in the Niger Delta *Int. J. Remote Sens.* **35** 1900–25

Asadi-Fard E, Falahatkar S, Tanha Ziyarati M, Zhang X and Faruolo M 2023 Assessment of RXD algorithm Capability for Gas Flaring detection through OLI-SWIR channels *Sustainability* **15** 1-20

Böttcher K, Paunu -V-V, Kupiainen K, Zhizhin M, Matveev A, Savolahti M, Klimont Z, Väätäinen S, Lamberg H and Karvosenoja N 2021 Black carbon emissions from flaring in Russia in the period 2012–2017 *Atmos. Environ.* **254** 118390

Carbon Limits AS 2016 Associated petroleum gas flaring study for egypt *Final report*

Caseiro A, Gehrke B, Rücker G, Leimbach D and Kaiser J W 2020 Gas flaring activity and black carbon emissions in 2017 derived from the Sentinel-3A sea and land surface temperature radiometer *Earth Syst. Sci. Data* **12** 2137–55

Caseiro A and Soszyńska A 2023 Quantification of gas flaring from satellite imagery: a comparison of two methods for SLSTR and BIROS imagery *J. Imaging* **9** 1-20

Chakraborty S, Oda T, Kalb V L, Wang Z and Román M O 2023 Potentially underestimated gas flaring activities—a new approach to detect combustion using machine learning and NASA's Black Marble product suite *Environ. Res. Lett.* **18** 1-12

Chaves M E D, Picoli M C A and Sanches I D 2020 Recent applications of landsat 8/OLI and sentinel-2/MSI for land use and land cover mapping: a systematic review *Remote Sens.* **12** 3062

Chowdhury S, Shipman T, Chao D, Elvidge C D, Zhizhin M and Hsu F C 2014 Daytime gas flare detection using Landsat-8 multispectral data *Proc. IEEE Int. Geoscience Remote Sensing Symp.* (*Quebec City, QC, Canada, 13–18 July 2014*) pp 258–61

Climate Action A 2023 Summary of global climate action at COP 28 (available at: https://unfccc.int/sites/default/files/resource/Summary_GCA_COP28.pdf)

Dubovik O, Schuster G L, Xu F, Hu Y, Bösch H, Landgraf J and Li Z 2021 Grand challenges in satellite remote sensing *Front. remote sens.* **2** 619818

Elvidge C D, Zhizhin M, Baugh K, Hsu F-C and Ghosh T 2016 Methods for global survey of natural gas flaring from visible infrared imaging radiometer suite data *Energies* **9** 14

Elvidge C D, Zhizhin M, Hsu F-C and Baugh K E 2013 VIIRS nightfire: satellite pyrometry at night *Remote Sens.* **5** 4423–49

Elvidge C D, Zhizhin M, Sparks T, Ghosh T, Pon S, Bazilian M, Sutton P, C and Miller S D 2023 Global satellite monitoring of exothermic industrial activity via infrared emissions *Remote Sens.* **15** 4760

Emam E A 2016 Environmental pollution and measurement of gas flaring *Int. J. Sci. Res. Sci. Eng. Technol.* **2** 252–62

Faruolo M, Caseiro A, Lacava T and Kaiser J 2021 Gas flaring: a review focused on its analysis from space *IEEE Geosci. Remote Sens. Mag.* **9** 258–81

Faruolo M, Coviello I, Filizzola C, Lacava T, Pergola N and Tramutoli V 2014 A satellite-based analysis of the Val d'Agri oil center (southern Italy) gas flaring emissions *Nat. Hazards Earth Syst. Sci.* **14** 2783–93

Faruolo M, Falconieri A, Genzano N, Lacava T, Marchese F and Pergola N 2022a A daytime multi-sensor satellite system for global gas flaring monitoring *IEEE Trans. Geosci. Remote* **60** 1–17

Faruolo M, Genzano N, Marchese F and Pergola N 2022b A tailored approach for the global gas flaring investigation by means of daytime satellite imagery *Remote Sens.* **14** 6319

Faruolo M, Genzano N, Marchese F and Pergola N 2023 Multi-temporal satellite investigation of gas flaring in Iraq and Iran: the DAFI porting on collection 2 LANDSAT 8/9 and sentinel 2A/B *Sensors* **23** 5734

Faruolo M, Lacava T, Pergola N and Tramutoli V 2020 The VIIRS-based RST-FLARE configuration: the Val d'Agri oil center gas flaring investigation in between 2015–2019 *Remote Sens.* **12** 819

Fawole O G, Cai X M and MacKenzie A R 2016 Gas flaring and resultant air pollution: a review focusing on black carbon *Environ. Pollut.* **216** 182–97

Flareintel 2021 Gas flaring threatens Algeria's energy exports to Europe (available at: https://flareintel.com/insights/gas-flaring-threatens-algerias-energy-exports-to-europe)

Genzano N, Pergola N and Marchese F 2020 A Google Earth engine tool to investigate, map and monitor volcanic thermal anomalies at global scale by means of mid-high spatial resolution satellite data *Remote Sens.* **12** 3232

Gorelick N, Hancher M, Dixon M, Ilyushchenko S, Thau D and Moore R 2017 Google earth engine: planetary-scale geospatial analysis for everyone *Remote Sens. Environ.* **202** 18–27

Hu C, Zhang X, Xing X and Gao Q 2023 An approach to detect gas flaring sites using sentinel-2 MSI and NOAA-20 VIIRS images *Int. J. Appl. Earth Obs. Geoinf.* **124** 103534

International Energy Agency (IEA) 2023 The oil and gas industry in net zero transitions. world energy outlook *Special Report* (available at: https://iea.blob.core.windows.net/assets/41800202-d427-44fa-8544-12e3d6e023b4/TheOilandGasIndustryinNetZeroTransitions.pdf)

Kumar L and Mutanga O 2018 Google earth engine applications since inception: usage, trends, and potential *Remote Sens.* **10** 1509

Liu Y, Pu Y, Hu X, Dong Y, Wu W, Hu C, Zhang Y and Wang S 2023 Global declines of offshore gas flaring inadequate to meet the 2030 goal *Nat. Sustain.* **6** 1095–102

Liu Y, Zhi W, Xu B, Xu W and Wu W 2021 Detecting high-temperature anomalies from Sentinel-2 MSI images *ISPRS J. Photogramm. Remote Sens.* **177** 174–93

Marchese F and Genzano N 2022 Global volcano monitoring through the NHI (Normalized Hotspot Indices) system *J. Geol. Soc.* **180** 1–13

Marchese F, Genzano N, Neri M, Falconieri A, Mazzeo G and Pergola N 2019 A multi-channel algorithm for mapping volcanic thermal anomalies by means of Sentinel-2 MSI and Landsat-8 OLI data *Remote Sens.* **11** 2876

Masek J G, Wulder M A, Markham B, McCorkel J, Crawford C J, Storey J and Jenstrom D T 2020 Landsat 9: empowering open science and applications through continuity *Remote Sens. Environ.* **248** 111968

Micijevic E, Barsi J, Haque M O, Levy R, Anderson C, Thome K, Czapla-Myers J and Helder D 2022 Radiometric performance of the landsat 9 operational land imager over the first 8 months on orbit *Proc. SPIE* **12232** 250–7

Naus S *et al* 2023 Assessing the relative importance of satellite-detected methane superemitters in quantifying total emissions for oil and gas production areas in Algeria *Environ. Sci. Technol.* **57** 19545–56

Onoda M and Young O R (eds) 2017 *Satellite Earth Observations and Their Impact on Society and Policy* (Springer) (https://doi.org/10.1007/978-981-10-3713-9)

The World Bank Global Flaring and Methane Reduction Partnership (GFMR) Briefs 2024 GGFR to evolve to the global flaring & methane reduction partnership (available at: www.worldbank.org/en/programs/gasflaringreduction/brief/ggfr-to-evolve-to-the-global-flaring-methane-reduction-partnership)

The World Bank 2023 Global gas flaring tracker report March 2023 (available at: https://thedocs.worldbank.org/en/doc/5d5c5c8b0f451b472e858ceb97624a18-0400072023/original/2023-Global-Gas-Flaring-Tracker-Report.pdf)

U.S. Geological Survey (USGS) 2020 Landsat collection 1 vs. collection 2 summary (available at: www.usgs.gov/media/files/landsat-collection-1-vs-collection-2-summary)

United Nations Climate Change Conference(UNFCCC) 2023 Oil & gas decarbonization charter launched to accelerate climate action (available at: www.cop28.com/en/news/2023/12/Oil-Gas-Decarbonization-Charter-launched-to–accelerate-climate-action)

Wilkinson R, Mleczko M M, Brewin R J W, Gaston K J, Mueller M, Shutler J D, Yan X and Anderson K 2024 Environmental impacts of earth observation data in the constellation and cloud computing era *Sci. Total Environ.* **909** 168584

Wu W *et al* 2022 Monitoring gas flaring in Texas using time-series Sentinel-2 MSI and Landsat-8 OLI images *Int. J. Appl. Earth Obs. Geoinf.* **114** 103075

Wulder M A, Hermosilla T, White J C, Hobart G and Masek J G 2021 Augmenting landsat time series with harmonized landsat sentinel-2 data products: assessment of spectral correspondence *Sci. Remote Sens.* **4** 100031

Ye W, Zhang F, He X, Bai Y, Liu R and Du Z 2020 A tile-based framework with a spatial-aware feature for easy access and efficient analysis of marine remote sensing data *Remote Sens.* **12** 1932

Zhizhin M, Matveev A, Ghosh T, Hsu F-C, Howells M and Elvidge C 2021 Measuring gas flaring in russia with multispectral VIIRS nightfire *Remote Sens.* **13** 3078